6

Acoustic Waves in Phononic Crystal Plates

Xin-Ye Zou, Xue-Feng Zhu, Bin Liang and Jian-Chun Cheng
Nanjing University,
People's Republic of China

1. Introduction

Recently, the study on elastic waves in phononic crystal plates is becoming a research hotspot due to its potential applications, especially in wireless communication, transducer and sensor system [1-10]. The phononic crystal plates commonly consist of two materials with large contrast in elastic properties and densities, arranging in a periodic (or quasiperiodic) array. The absolute band gaps in composite plates can forbid the propagation of all elastic wave modes in all directions. Comparing with the bulk wave and surface acoustic wave devices, phononic crystal plates have better performance in elastic wave propagation since the phase speed of most Lamb wave modes (except for A_0 mode) is faster than surface wave mode, and also the wave energy in plates is totally confined between the upper and nether free-stress boundaries regardless of the air damp and self-dissipation, which provides a special potentiality in micro-electronics in wireless communication.

The propagation of Lamb waves is much more complicated than bulk wave and surface acoustic wave in terms of the free-stress boundaries which can couple the longitudinal and transversal strain components. The first attempt to describe the propagation of Lamb waves with wavelength comparable with the lattice is due to Auld and co-workers [11-12], who studied 2D composites within the couple-mode approximation. Alippi et al. [13] have presented an experimental study on the stopband phenomenon of lowest-order Lamb waves in piezoelectric periodic composite plates and interpreted their results in terms of a theoretical model, which provides approximate dispersion curves of the lowest Lamb waves in the frequency range below the first thickness mode by assuming no coupling between different Lamb modes. The transmissivity of the finite structure to Lamb wave modes was also calculated by taking into account the effective plate velocities of the two constituent materials [14]. Based on a rigorous theory of elastic wave, Chen et al.[1] have employed plane wave expansion (PWE) method and transient response analysis (TRA) to demonstrate the existence of stop bands for lower-order Lamb wave modes in 1D plate. Gao et al.[8] have developed a virtual plane wave expansion (V-PWE) method to study the substrate effect on the band gaps of lower-order Lamb waves propagating in thin plate with 1D phononic crystal coated on uniform substrate. They also studied the quasiperiodic (Fibonacci system) 1D system and find out the existence of split in phonon band gap [2]. In order to reduce the computational complexity without losing the accuracy, Zhu et al.[9] have promoted an efficient method named harmony response analysis (HRA) and supercell plane wave expansion (SC PWE) to study the behavior of Lamb wave in silicon-based 1D composite plates. Zou et al.[10] have employed V-PWE method to study the band gaps of plate-mode waves in 1D piezoelectric composite plates with substrates.

Source: Acoustic Waves, Book edited by: Don W. Dissanayake,
ISBN 978-953-307-111-4, pp. 466, September 2010, Sciyo, Croatia, downloaded from SCIYO.COM

The chapter is structured as follows: we firstly introduce the theory and modeling used in this chapter in Section 2. In Section 3, we focus on the band gaps of lower-order Lamb waves in 1D composite thin plates without/with substrate. In Section 4, we study the lamb waves in 1D quasiperiodic composite thin plates. In Section 5, we focus on acoustic wave behavior in silicon-based 1D phononic crystal plates for different structures, and finally in Section 6, we study the band gaps of plate-mode waves in 1D piezoelectric composite plates without/with substrates.

2. Theory and modeling of phononic crystal plates

In this section, we give the theory and modeling of phononic crystal plates with different structures: the periodic structure without/with substrate, and the quasiperiodic structure.

2.1 Periodic structure without substrate by PWE method

As shown in Fig. 1, the periodic composite plate consists of material A with width d_A, material B with d_B, lattice spacing $D = d_A + d_B$, and filling rate defined by $f = d_A / D$. The wave propagates along the x direction of a plate bounded by planes $z = 0$ and $z = L$.

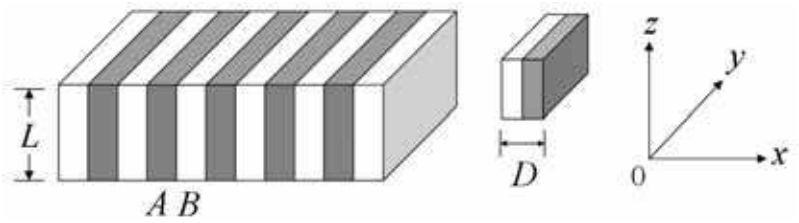

Fig. 1. 1D periodic composite plate consisting of alternate A and B strips.

In the periodic structure, all field components are assumed to be independent of the y direction. In an inhomogeneous linear elastic medium with no body force, the equation of motion for displacement vector $\boldsymbol{u}(x,z,t)$ can be written as

$$\rho(x)\ddot{\boldsymbol{u}}_p = \partial_q[c_{pqmn}(x)\partial_n \boldsymbol{u}_m], \quad (p = 1,2,3), \tag{1}$$

where $\rho(x)$ and $c_{pqmn}(x)$ are the x-dependent mass density and elastic stiffness tensor, respectively. Due to the spatial periodicity in the x direction, the material constants, $\rho(x)$ and $c_{pqmn}(x)$ can be expanded in the Fourier series with respect to the 1D reciprocal lattice vectors (RLVs), as follows

$$\rho(x) = \sum_G e^{jGx}\rho_G, \tag{2}$$

$$c_{pqmn}(x) = \sum_G e^{jGx}c^G_{pqmn}, \tag{3}$$

where ρ_G and c^G_{pqmn} are expansion coefficients of the mass density and elastic stiffness tensor, respectively. From the Bloch theorem and by expanding the displacement vector $\boldsymbol{u}(x,z,t)$ into Fourier series, one obtains

$$\boldsymbol{u}(x,z,t)=\sum_{G} e^{jk_x x-j\omega t}(e^{jGx}\boldsymbol{A}_G e^{jk_z z}), \tag{4}$$

where k_x is a Bloch wave vector and ω is the circular frequency, $\boldsymbol{A}_G=(A_G^1,A_G^2,A_G^3)$ is the amplitude vector of the partial waves, and k_z is the wave number of the partial waves along the z direction. Substituting Eqs. (2)-(4) into Eq. (1), one obtains homogenous linear equations to determine both (A_G^1,A_G^2,A_G^3) and k_z.

$$\begin{pmatrix} c_{11}(k_x+G)(k_x+G')+c_{44}k_z^2-\rho\omega^2 & 0 & c_{12}(k_x+G)+c_{44}(k_x+G')k_z \\ 0 & c_{44}(k_x+G)(k_x+G')+c_{44}k_z^2-\rho\omega^2 & 0 \\ c_{12}(k_x+G')+c_{44}(k_x+G)k_z & 0 & c_{44}(k_x+G)(k_x+G')+c_{11}k_z^2-\rho\omega^2 \end{pmatrix}\begin{pmatrix} A_{G'}^1 \\ A_{G'}^2 \\ A_{G'}^3 \end{pmatrix}=0, \tag{5}$$

Supposing that the materials *A* and *B* are cubic materials, it is obvious that the wave motion polarized in the *y*-direction, namely SH wave, decouples to the wave motions polarized in the *x*- and *z*-directions, namely, P and SV waves. It is relatively simple to discuss the SH wave so that we focus our attentions to P and SV waves, and the equation of motion for Lamb waves becomes

$$\begin{pmatrix} c_{11}(k_x+G)(k_x+G')+c_{44}k_z^2-\rho\omega^2 & c_{12}(k_x+G)+c_{44}(k_x+G')k_z \\ c_{12}(k_x+G')+c_{44}(k_x+G)k_z & c_{44}(k_x+G)(k_x+G')+c_{11}k_z^2-\rho\omega^2 \end{pmatrix}\begin{pmatrix} A_{G'}^1 \\ A_{G'}^3 \end{pmatrix}=0, \tag{6}$$

If one truncates the expansions of Eqs. (2) and (3) by choosing n RLVs, one will obtain $4n$ eigenvalues $k_z^{(l)}$, $(l=1-4n)$. For the Lamb waves, all of the $4n$ eigenvalues $k_z^{(l)}$ must be included. Accordingly, displacement vector of the Lamb waves can be taken of the form

$$\boldsymbol{u}(x,z,t)=\sum_{G}{}' e^{i(k_x+G)x-i\omega t}\left(\sum_{l=1}^{4n}\boldsymbol{A}_G e^{iK_z^{(l)}z}\right)=\sum_{G}{}' e^{i(k_x+G)x-i\omega t}\left(\sum_{l=1}^{4n}X_l\varepsilon_G^{(l)}e^{ik_z^{(l)}z}\right), \tag{7}$$

where $\varepsilon_G^{(l)}$ is the associated eigenvector for the eigenvalue $k_z^{(l)}$, X_l is the weighting coefficient to be determined, and the prime of the summation expresses that the sum over G is truncated up to n.

The boundary conditions are the stress-free on the upper (z = 0) and rear (z = L) surfaces

$$\boldsymbol{T}_{p3}\big|_{z=0,L}=c_{p3mn}\partial_n u_m\big|_{z=0,L}=0 \qquad (p=1,3). \tag{8}$$

which $\boldsymbol{T}_{p3}$ is the stress tensor and L is the plate thickness. Eq. (8) leads to $4n$ homogeneous linear equations for X_l l = (1- $4n$), as follows

$$\begin{bmatrix} H_{1,G}^{(1)} & H_{1,G}^{(2)} & \cdots & H_{1,G}^{(4n)} \\ H_{2,G}^{(1)} & H_{2,G}^{(2)} & \cdots & H_{2,G}^{(4n)} \\ H_{3,G}^{(1)} & H_{3,G}^{(2)} & \cdots & H_{3,G}^{(4n)} \\ H_{4,G}^{(1)} & H_{4,G}^{(2)} & \cdots & H_{4,G}^{(4n)} \end{bmatrix}\begin{bmatrix} X_1 \\ X_2 \\ \vdots \\ X_{4n} \end{bmatrix}=\tilde{H}X=0, \tag{9}$$

where $\tilde{H}$ is a $4n \times 4n$ matrix with components

$$H_{1,G}^{(l)} = C_{G-G'}^{44}[(k_x + G')\varepsilon_{G'}^{3(l)} + k_z^{(l)}\varepsilon_{G'}^{1(l)}], \tag{10a}$$

$$H_{2,G}^{(l)} = C_{G-G'}^{11} k_z^{(l)} \varepsilon_{G'}^{3(l)} + C_{G-G'}^{12}(k_x + G')\varepsilon_{G'}^{1(l)}, \tag{10b}$$

$$H_{3,G}^{(l)} = C_{G-G'}^{44}[(k_x + G')\varepsilon_{G'}^{3(l)} + k_z^{(l)}\varepsilon_{G'}^{1(l)}] \times \exp(jk_z^{(l)}L), \tag{10c}$$

$$H_{4,G}^{(l)} = [C_{G-G'}^{11} k_z^{(l)} \varepsilon_{G'}^{3(l)} + C_{G-G'}^{12}(k_x + G')\varepsilon_{G'}^{1(l)}] \times \exp(jk_z^{(l)}L). \tag{10d}$$

From Eq. (9) one notes that to obtain nontrivial solution for the X_l, the determinant of the boundary condition matrix should be equal to zero. The ω of the Lamb wave modes are thus found by searching for the values of ω that simultaneously make the Eq. (6) and $\det(\tilde{H})$ equal to zero. In practice, an iterative search procedure is usually required to find these ω [15-16].

2.2 Periodic structure with substrate by V-PWE method

As shown in Fig.2, the composite plate with substrate consists of the 1D phononic crystal (PC) layer coated on C substrate. The PC layer consists of the material A with the width d_A and the material B with the width d_B.

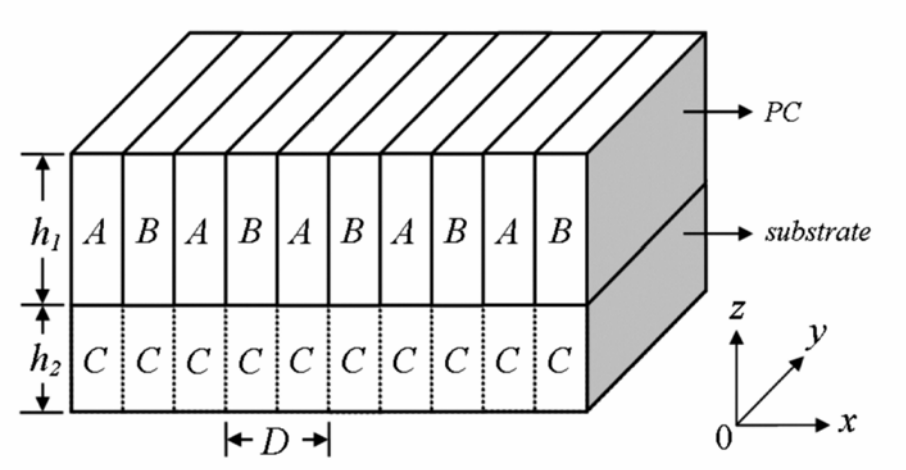

Fig. 2. The 1D periodic composite plate consisting of alternate A and B strips with a substrate C.

We develop a V-PWE method to calculate the dispersion curves of Lamb wave modes propagating along the x direction in the presence of the uniform substrate. Here, we give the equations of V-PWE method for the piezoelectric periodic structure with substrate. One can have the equations for non-piezoelectric situation by omitting the piezoelectricity components and the electrical boundary conditions.

In the situation of piezoelectric composite plate with substrate, the equations governing the motion of lattice displacement $\boldsymbol{u}^m(x,z,t)$ and electrical displacement $\boldsymbol{D}^m(x,z,t)$ in this inhomogeneous system are given by

$$\rho^m(x)\ddot{u}_j^m = \partial_i T_{ij}^m, \tag{11}$$

$$\partial_i D_i^m = 0, \tag{12}$$

$$T_{ij}^m = c_{ijkl}^m(x)\partial_l u_k^m + e_{lij}^m(x)\partial_l \phi^m, \tag{13}$$

$$D_i^m = e_{ikl}^m(x)\partial_l u_k^m - \varepsilon_{il}^m(x)\partial_l \phi^m, \tag{14}$$

where $i,j,k,l = x,z;\ m = 1,2$ (1 represents phononic layer; 2 represents the substrate, respectively). $\boldsymbol{T}_{ij}^m(x,z,t)$, $\boldsymbol{D}^m(x,z,t)$, $\boldsymbol{u}^m(x,z,t)$, $\varphi^m(x,z,t)$, $\rho^m(x)$, $c_{ijkl}^m(x)$, $e_{lij}^m(x)$, and $\varepsilon_{il}^m(x)$ are the stress vector, electrical displacement vector, displacement vector, electric potential, x-dependent mass density, elastic stiffness, piezoelectric, and dielectric constant tensors, respectively. It comes into notice that in fact the material constants depend on the z-direction due to the existence of the substrate, as follows

$$\alpha(x,z) = \begin{cases} \alpha^1(x), & (0 < z < h_1) \\ \alpha^2, & (-h_2 < z < 0) \end{cases} \tag{15}$$

where $\alpha = (\rho, c_{ijkl}, e_{lij}, \varepsilon_{il})$, $(\rho^2, c_{ijkl}^2, e_{lij}^2, \varepsilon_{il}^2)$ are the material constants for the substrate.

Due to the spatial periodicity, the Bloch theorem can be applied to the PC layer, but it cannot be simply applied to the substrate layer. However, one notice that the triangle basic function set in the Fourier series is an orthogonal and complete set, each components in the Fourier series must satisfied the boundary conditions at the interface between the PC layer and the substrate at $z = 0$, namely the continuities of the normal stress, normal displacement, normal electrical displacement and electric potential.

$$T_{iz}^1\Big|_{z=0} = T_{iz}^2\Big|_{z=0},\ u_{iz}^1\Big|_{z=0} = u_{iz}^2\Big|_{z=0},\ D_z^1\Big|_{z=0} = D_z^2\Big|_{z=0},\ \phi^1\Big|_{z=0} = \phi^2\Big|_{z=0},\ (i = x,z). \tag{16}$$

Therefore, the displacement and electric potential fields in the substrate layer also must be expanded to the Fourier series with the period that is same as the PC layer in order to satisfy the boundary conditions. Then the substrate layer can be treated as a virtual periodic structure that has the same filling fraction and period as the PC layer. Thereupon, the Bloch theorem can be applied to both the PC and the substrate layers.

Due to the spatial periodicity in the x direction, the material constants can be expanded in Fourier series with respect to the 1-D reciprocal-lattice vector (RLV) G, as follows:

$$\alpha(x) = \sum_G e^{jGx}\alpha_G, \tag{17}$$

where α_G is the corresponding Fourier coefficient. Utilizing the Bloch theorem and expanding the displacement vector and electric potential into Fourier series in the PC and the substrate layers, one obtains

$$\boldsymbol{u}^m(x,z,t) = \sum_G e^{j(k_x x-\omega t)}(e^{jGx}\mathrm{A}_G^m e^{jk_z^m z}), \tag{18}$$

$$\phi^m(x,z,t) = \sum_G e^{j(k_x x-\omega t)}(e^{jGx}A_{G3}^m e^{jk_z^m z}), \tag{19}$$

where k_x is a Bloch wave vector, ω is the circular frequency, and k_z^m is the wave number along the *z*-direction, $A_G^m = (A_{G1}^m, A_{G2}^m)$ and A_{G3}^m are the amplitude vectors of the partial waves and electric potential, respectively. Substituting Eqs. (17)-(19) into Eqs. (11)-(14), one can obtain the eigenvalue problem with respect to k_z^m:

$$(\boldsymbol{A}^m k_z^{m2} + \boldsymbol{B}^m k_z^m + \boldsymbol{C}^m)\cdot \mathrm{U}^m = 0, \tag{20}$$

where $\boldsymbol{U}^m = \{A_{G1}^m, A_{G2}^m, A_{G3}^m\}^T$ is called the generalized displacement vector, the $3n\times 3n$ matrices $\boldsymbol{A}^m$, $\boldsymbol{B}^m$, and $\boldsymbol{C}^m$ are functions of k_x, G, ω, ρ_G^m, $c_G^{ijkl m}$, $e_G^{lij m}$, $\varepsilon_G^{il m}$, and n is the number of RLV.

Here, we consider the stress-free boundary conditions and two kinds of the electrical boundary conditions. For the 1-D problem, we have

the stress free boundary conditions:

$$T_{iz}^1\Big|_{z=h_1} = 0, \quad T_{iz}^2\Big|_{z=-h_2} = 0, \quad (i = x,z), \tag{21}$$

the OC boundary conditions:

$$D_z^1\Big|_{z=h_1} = D_z^{air}\Big|_{z=h_1}, \quad \phi^1\Big|_{z=h_1} = \phi^{air}\Big|_{z=h_1},$$

$$D_z^2\Big|_{z=-h_2} = D_z^{air}\Big|_{z=-h_2}, \ \phi^2\Big|_{z=-h_2} = \phi^{air}\Big|_{z=-h_2}, \tag{22}$$

$$(D_z^{air} = -\varepsilon_0\frac{\partial\phi^{air}}{\partial z}, \quad \varepsilon_0 = 1\times 10^{-11}\mathrm{F/m},)$$

the SC boundary conditions:

$$\phi^1\Big|_{z=h_1} = 0, \qquad \phi^2\Big|_{z=-h_2} = 0. \tag{23}$$

Putting $A_G^{j(l)m} = X_l^m \beta_G^{j(l)m}$ ($j = 1-3$, $l = 1-6n$, $m = 1,2$), where $\beta_G^{j(l)m}$ is the associated eigenvector of the eigenvalue $k_z^{(l)m}$, and X_l^m is the weighting coefficient that can be determined from the boundary conditions for different layers, one obtains: $\mathbf{H}\cdot\mathbf{X} = 0$ from the equations (16), (21) and (22) [or (23)], where $\mathbf{H}$ is a $12n\times 12n$ matrix. The existence of a nontrivial solution of X_l^m needs the determinant of matrix $\mathbf{H}$ to be zero

$$\det(\mathbf{H}) = 0. \tag{24}$$

Then one can obtain the dispersion relations of the Lamb waves propagating in a 1-D PC layer coated on a substrate.

2.3 Periodic structure without/with substrate by FE method

In order to study the elastic wave in the phononic crystal plates, transient response analysis (TRA) and the harmony response analysis (HRA) are presented here by finite element (FE) method.

First, the TRA is employed to calculate the transmitted power spectra (TPS) for the finite periodic structure. The FE solution involves the discretization of the domain into a number of elements, approximating the displacement values interior to the elements in term of its nodal value through the shape functions of the chosen element and the determination of nodal values [17].

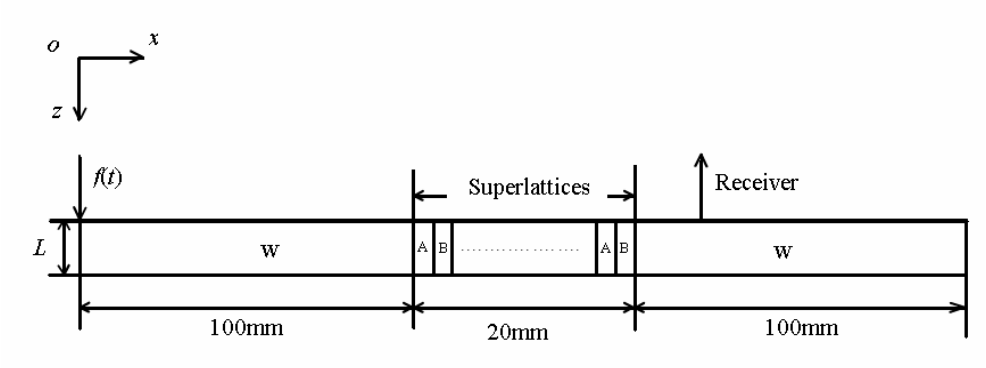

Fig. 3. Modified plate geometry in the Finite Element calculations

Fig. 3 shows the configuration of the modified composite plate in the Finite Element calculations, in which the superlattices with ten periods (the length is 20 mm) is bounded by two pure tungsten plates (the length is 100 mm) at two sides. Lamb waves are excited by the force function $f(t)$ that is a triangle wave at $x = 0$, and are received at $x = 140$ mm [18]. The generation source is far from the periodic structure in order to obtain approximate plane waves when the wavefronts reach it. The step sizes of temporal and spatial discretization in the finite model are fine enough for the convergence of the numerical results (increasing the number of elements of the finite element mesh is equivalent to increasing the number of harmonics in PWE method). The vertical displacement of a node at upper surface of the plate behind the superlattices array at $x = 140$ mm is collected as function of time. For a sufficiently large number of these vertical displacement data on the time axis, the displacement fields are Fourier transformed into the frequency domain to yield the TPS.

We also promote an efficient method named HRA to study the propagation and transmission of acoustic waves in 1D phononic crystal plates. Comparing with TRA [1,2,8], HRA is more time-saving due to its direct calculation in frequency domain and more powerful for the acquirability of displacement field under certain frequency load, which can be further employed to the designation of various phononic crystal functionalities such as filters, resonators and waveguides. With this method, we can study the cases both without and with substrates. Taking the gradient of the displacement fields, we can further study the strain distribution in the plates, and it is really a very direct way to understand how the band gaps form in phononic crystal plates by comparing displacement fields under different frequency loads (inside/outside band gaps).

Any continual periodic loads can produce continual periodic response (harmony response) in phononic crystal plates. HRA is a method used to define the stabilized response of linear structures under time-harmonic loads. By calculating the responses (usually displacement fields) under different frequency loads, we can obtain the transmitted power spectra in the detected region. HRA is a linear analysis regardless of any nonlinear characteristics. For multi-element structure, the Newton's second law can be expressed as follows:

$$[\boldsymbol{M}]\{\ddot{\boldsymbol{D}}\}+[\boldsymbol{C}]\{\dot{\boldsymbol{D}}\}+\{\boldsymbol{R}^{int}\}=\{\boldsymbol{R}^{ext}\} \tag{25a}$$

$$\{\boldsymbol{R}^{int}\}=[\boldsymbol{K}]\{\boldsymbol{D}\} \tag{25b}$$

$$\{\boldsymbol{R}^{ext}\}=\{\boldsymbol{F}\}\exp(i\Omega t) \tag{25c}$$

where $[\boldsymbol{M}]$, $[\boldsymbol{C}]$ and $[\boldsymbol{K}]$ are general mass matrix, damping matrix and stiffness matrix, respectively; $\{\boldsymbol{D}\}$ and $\{\boldsymbol{F}\}\exp(i\Omega t)$ are nodal degree of freedom vector and nodal external load vector, respectively. Eq (25a) describes a dynamic balance among inertial force, damping force, inner force $\{\boldsymbol{R}^{int}\}$ and external load force $\{\boldsymbol{R}^{ext}\}$. The forced vibration of the structure will finally come to a stabilized status in which every node moves in harmonic motion with the same frequency (Ω). Further, we can express $\{\boldsymbol{D}\}$ into:

$$\{\boldsymbol{D}\}=\{\bar{\boldsymbol{D}}\}\exp(i\Omega t) \tag{26}$$

where $\{\bar{\boldsymbol{D}}\}$ is the complex nodal degree of freedom vector. By substituting Eq (26) into Eqs (25a)-(25c), we can obtain:

$$\left([\boldsymbol{K}]+i\Omega[\boldsymbol{C}]-\Omega^2[\boldsymbol{M}]\right)\{\bar{\boldsymbol{D}}\}=\{\boldsymbol{F}\} \tag{27}$$

where $\{\bar{\boldsymbol{D}}\}$ can be obtained using Frontal solver. We choose imaginary component of $\{\bar{\boldsymbol{D}}\}$ to build up the stabilized displacement field under different frequency loads. It is necessary to mention that TRA requires much more substeps to obtain the nodal degree of freedom vector at certain detected time for the reason that the time step Δt should obey the following criterion for numerical convergence in Newmark method: [19]

$$\Delta t \le \frac{\Omega_{crit}}{2\pi f_{max}} \tag{28}$$

where f_{max} is the maximum frequency of interest. Ω_{crit} is defined to be:

$$\Omega_{crit}=\left(\frac{\gamma}{2}-\beta\right)^2 \tag{29}$$

where β is chosen to be $(\gamma+1/2)^2/4$ with $\gamma \ge 1/2$ to achieve as large high frequency dissipation as possible. We choose $\beta=0.2756$, $\gamma=0.55$ in the numerical calculation of TRA. In each substep, a very complex iteration is employed, which takes the form:

$$\left[\boldsymbol{K}^{eff}\right]\{\boldsymbol{D}\}_{n+1}=\left\{\boldsymbol{R}^{ext}\right\}_{n+1}+[\boldsymbol{M}]\left(\frac{\{\boldsymbol{D}\}_{n+1}}{\beta\Delta t^2}+\frac{\{\dot{\boldsymbol{D}}\}_n}{\beta\Delta t}+\frac{\{\ddot{\boldsymbol{D}}\}_n(1-2\beta)}{2\beta}\right)$$
$$+[\boldsymbol{C}]\left(\frac{\{\boldsymbol{D}\}_n\gamma}{\beta\Delta t}+\frac{\{\dot{\boldsymbol{D}}\}_n(\gamma-\beta)}{\beta}+\frac{\{\ddot{\boldsymbol{D}}\}_n\Delta t(\gamma-2\beta)}{2\beta}\right) \tag{30a}$$

$$\{\dot{\boldsymbol{D}}\}_{n+1}=\frac{(\{\boldsymbol{D}\}_{n+1}-\{\boldsymbol{D}\}_n)\gamma}{\beta\Delta t}-\frac{\{\dot{\boldsymbol{D}}\}_n(\gamma-\beta)}{\beta}-\frac{\{\ddot{\boldsymbol{D}}\}_n\Delta t(\gamma-2\beta)}{2\beta} \tag{30b}$$

$$\{\ddot{\boldsymbol{D}}\}_{n+1}=\frac{(\{\boldsymbol{D}\}_{n+1}-\{\boldsymbol{D}\}_n-\Delta t\{\dot{\boldsymbol{D}}\}_n)}{\beta\Delta t^2}-\frac{\{\ddot{\boldsymbol{D}}\}_n(1-2\beta)}{2\beta} \tag{30c}$$

where $\left[\boldsymbol{K}^{eff}\right]=[\boldsymbol{M}]/(\beta\Delta t^2)+[\boldsymbol{C}]\gamma/(\beta\Delta t)+[\boldsymbol{K}]$. The initial condition for Eqs (30a)-(30c) is shown as follows:

$$\{\ddot{\boldsymbol{D}}\}_0=[\boldsymbol{M}]^{-1}\left(\left\{\boldsymbol{R}^{ext}\right\}_0-[\boldsymbol{K}]\{\boldsymbol{D}\}_0-[\boldsymbol{C}]\{\dot{\boldsymbol{D}}\}_0\right) \tag{31}$$

With Eqs (30a)-(30c) and (31), we can obtain $\{\boldsymbol{D}\}_1$, $\{\boldsymbol{D}\}_2$, $\{\boldsymbol{D}\}_3$, and so forth. From the above-mentioned details, it is obvious that the numerical calculation of TRA is more complicated than that of HRA and therefore requires more computation resources when the model being larger.

In TRA or HRA, we need to suppress reflections from the hard boundary to get rid of the unwanted resonance peaks. Based on the wave equation in spherical coordinate, artificial boundary can be equivalent to many continuous distribution parallel viscous-spring systems. The coefficients of stiffness and damping are given as follows:

$$K_T=\frac{\alpha_T G}{LN};\ K_N=\frac{\alpha_N G}{LN} \tag{32a}$$

$$C_T=\frac{\sqrt{G\rho}}{N};\ C_N=\frac{\sqrt{E\rho}}{N} \tag{32b}$$

where K_T and K_N are tangential and normal stiffness coefficients of springs, respectively; ρ is the material density of matrix silicon; C_T and C_N are tangential and normal damping coefficients, respectively; G and E are shear modulus and Young's modulus of matrix silicon, respectively; L and N are the distance from exciting source to artificial boundary and number of viscous-spring systems attached to the boundary, respectively; α_T and α_N are the tangential and normal modified coefficients for artificial boundary, respectively. α_T and α_N are assigned with 0.67 and 1.33, respectively [20].

2.4 Periodic structure without/with Substrate by SC-PWE method

The super-cell plane wave expansion (SC-PWE) method is another efficient way to calculate the plate-mode waves of the phononic crystal plates. As shown in Fig. 4, we establish a 3D

model in Cartesian coordination to calculate the elastic band structures of 1D phononic crystal plates, where the periodic composite plate consists of alternate A and B strips, C is the LIM layer, and D is the substrate, respectively [21].

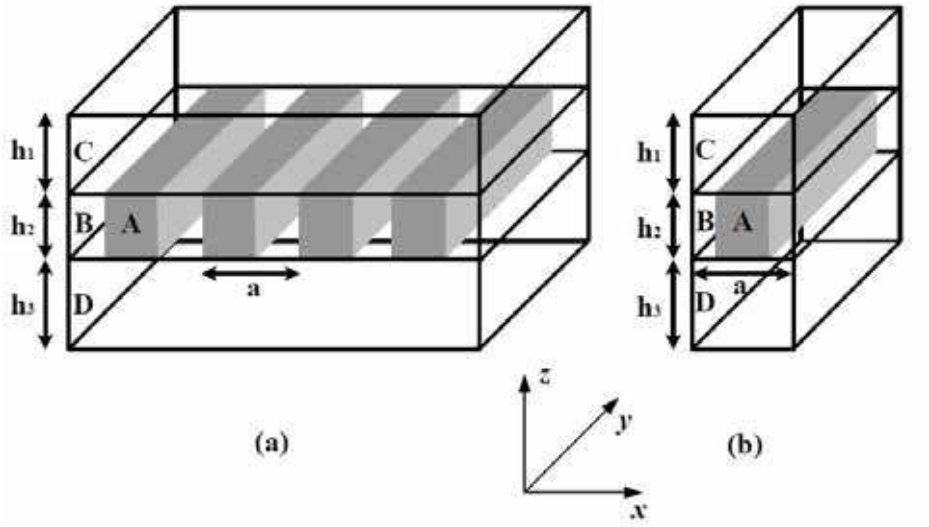

Fig. 4. (a) 1D Lamb wave phononic crystal plate sandwiched between two layers of homogeneous materials, and (b) 3D super-cell used in the computation.

The LIM is an imaginary material with relatively low elastic moduli for approximately meeting the requirement of free boundary condition and an extremely low mass density, which leads the sound speed in the LIM to be much larger than that in usual solid material. In this chapter, the LIM is assumed as an isotropic material with $C_{11} = 2 \times 10^6$ N/m², $C_{44} = 1 \times 10^6$ N/m², $C_{12} = 0$ N/m² and $\rho = 1 \times 10^{-4}$ kg/m³. The choice of such unphysical high sound speeds for the LIM is in good agreement with the numerical condition derived by Tanaka et al [22]. With these values, both good numerical convergence and computing accuracy can be achieved. The thickness of plate h is assumed to be 2 mm and $h = h_2 + h_3$ where $h_3 = 0$ mm for the case without substrate. The thickness of the LIM layer h_1 is defined to be $5h_2$ to reduce unexpected wave coupling between two nearest phononic layers in z direction [23]. In the absence of body force and strain in y direction, the SH mode wave in 1D plate can be decoupled. Regardless of the wave propagating in y direction, the elastic wave equations of phononic crystal are given by:

$$\rho(\boldsymbol{r})\ddot{u}_p = \partial_q[C_{pqmn}(\boldsymbol{r})\partial_n u_m] \quad (p = 1,2,3) \tag{33}$$

where $\boldsymbol{r} = (x,z)$. This equation can be solved by a standard Fourier expansion to $\rho(\boldsymbol{r})$, $C_{pqmn}(\boldsymbol{r})$ and $u(\boldsymbol{r},t)$, which are all position-dependent values. For convenience, we put $\alpha = (\rho, C_{pqmn})$ and then we can obtain the following equations:

$$\alpha(\boldsymbol{r}) = \sum_{\mathbf{G}_x}\sum_{G_z} \alpha_{\mathbf{G}} \exp[i(G_x x + G_z z)] \tag{34}$$

$$u(\boldsymbol{r},t)=\sum_{\boldsymbol{G}_x}\sum_{G_z}u_{\boldsymbol{G}}\exp[i(G_x x+G_z z)]e^{i(\boldsymbol{k}\cdot\boldsymbol{r}-\omega t)} \tag{35}$$

where $\boldsymbol{k}=(k_x,k_z)$ is the Bloch wave vector and the 2D reciprocal-lattice vector $\boldsymbol{G}=(G_x,G_z)$, respectively. Substituting equations (34) and (35) into wave equation (33), we can obtain:

$$\omega^2\begin{pmatrix}\rho_{\boldsymbol{G}-\boldsymbol{G}'} & & \\ & \rho_{\boldsymbol{G}-\boldsymbol{G}'} & \\ & & \rho_{\boldsymbol{G}-\boldsymbol{G}'}\end{pmatrix}u_{\boldsymbol{G}'}=\begin{pmatrix}M^{11}_{\boldsymbol{G},\boldsymbol{G}'} & M^{12}_{\boldsymbol{G},\boldsymbol{G}'} & M^{13}_{\boldsymbol{G},\boldsymbol{G}'}\\ M^{21}_{\boldsymbol{G},\boldsymbol{G}'} & M^{22}_{\boldsymbol{G},\boldsymbol{G}'} & M^{23}_{\boldsymbol{G},\boldsymbol{G}'}\\ M^{31}_{\boldsymbol{G},\boldsymbol{G}'} & M^{32}_{\boldsymbol{G},\boldsymbol{G}'} & M^{33}_{\boldsymbol{G},\boldsymbol{G}'}\end{pmatrix}u_{\boldsymbol{G}'} \tag{36a}$$

The explicit expressions of the matrix elements $M^{lm}_{\boldsymbol{G},\boldsymbol{G}'}$, ($l=m=1-3$) are:

$$\begin{aligned}
&M^{11}_{\boldsymbol{G},\boldsymbol{G}'}=C^{11}_{\boldsymbol{G}-\boldsymbol{G}'}(k_x+G'_x)(k_x+G_x)+C^{44}_{\boldsymbol{G}-\boldsymbol{G}}G'_zG_z \qquad M^{12}_{\boldsymbol{G},\boldsymbol{G}'}=0\\
&M^{13}_{\boldsymbol{G},\boldsymbol{G}'}=C^{12}_{\boldsymbol{G}-\boldsymbol{G}}G'_z(k_x+G_x)+C^{44}_{\boldsymbol{G}-\boldsymbol{G}'}(k_x+G'_x)G_z \qquad M^{21}_{\boldsymbol{G},\boldsymbol{G}'}=0\\
&M^{22}_{\boldsymbol{G},\boldsymbol{G}'}=C^{44}_{\boldsymbol{G}-\boldsymbol{G}'}(k_x+G'_x)(k_x+G_x)+C^{44}_{\boldsymbol{G}-\boldsymbol{G}}G'_zG_z \qquad M^{23}_{\boldsymbol{G},\boldsymbol{G}'}=0\\
&M^{31}_{\boldsymbol{G},\boldsymbol{G}'}=C^{44}_{\boldsymbol{G}-\boldsymbol{G}}G'_z(k_x+G_x)+C^{12}_{\boldsymbol{G}-\boldsymbol{G}'}(k_x+G'_x)G_z \qquad M^{32}_{\boldsymbol{G},\boldsymbol{G}'}=0\\
&M^{33}_{\boldsymbol{G},\boldsymbol{G}'}=C^{44}_{\boldsymbol{G}-\boldsymbol{G}'}(k_x+G'_x)(k_x+G_x)+C^{11}_{\boldsymbol{G}-\boldsymbol{G}}G'_zG_z
\end{aligned} \tag{36b}$$

where the Fourier coefficients $C^{pq}_{\boldsymbol{G}-\boldsymbol{G}'}$ are related to $C_{pqmn}(\boldsymbol{r})$ in a conventional manner. As shown in equation (36a), characteristic frequency ω is exactly the squared generalized eigenvalue of density matrix and elastic constant matrix. The coefficients $C^{pq}_{\boldsymbol{G}-\boldsymbol{G}'}$ and $\rho_{\boldsymbol{G}-\boldsymbol{G}'}$ takes the form:

$$\alpha_{\boldsymbol{G}-\boldsymbol{G}'}=\frac{1}{V_c}\iiint_{(Supercell)}\alpha(\boldsymbol{r})\exp[-i(\boldsymbol{G}-\boldsymbol{G}')\cdot\boldsymbol{r}]d^3\boldsymbol{r} \tag{37}$$

where V_c is the volume of super-cell. With the above-mentioned equations, we can easily obtain the band structure of 1D phononic crystal plate.

2.5 Quasiperiodic structure by FE method

As shown in Fig.5, the quasiperiodic composite plate consists of material A of width d_A and material B of width d_B. The lattice spacing is $D=d_A+d_B$. When the distribution of materials A and B is arranged according to the Fibonacci sequence, one obtains a quasiperiodic system [24]. We create the Fibonacci sequence *B*, *BA*, *BAB*, *BABBA*, *BABBABAB*, *BABBABABBABBA*, … according to the production rule $S_j=S_{j-1}|S_{j-2}$ for $j\geq 3$ with $S_1=B$ and $S_2=BA$. When A and B are put along the chain alternately, a periodic model is obtained. We introduce parameter $\Phi=d_A/d_B$ to describe the ratio of the two components. Φ is fixed at 1.0 and the number of layers N is 13 throughout the section unless otherwise stated. The wave propagates along the x direction of the plate bounded by planes $z=0$ and $z=L$. We consider a 2D problem, in which all field components are assumed to be y independent.

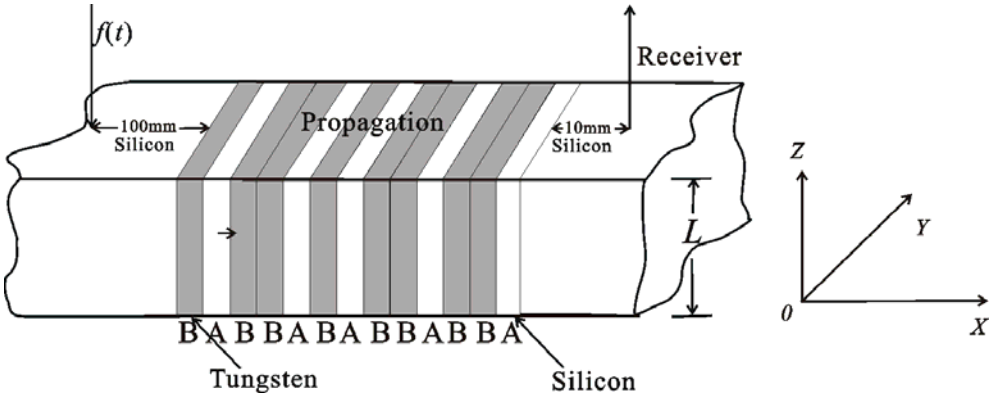

Fig. 5. The configuration of 1D quasiperiodic composite plate consisting of Tungsten and Silicon strips arranged following the Fibonacci sequence.

To demonstrate the structures of the band gaps for Lamb waves in the 1D quasiperiodic systems and the difference from that of periodic systems, we calculate TPS of the transient Lamb waves by using the TRA. We suppose that a Lamb wave is excited by a line laser pulse with a spatial Gaussian distribution (Gaussian radius = 0.2 mm). The laser pulse, which is normally incident to the surface of the studied plates, generates the Lamb wave propagating along the x direction. The laser-generated force source $f(t)$ is simulated as a delta function, which is perpendicular to the surface of the plate [25].

The elastic properties of the materials in the numerical calculations are the same as mentioned in above sections; and the thickness of the plates (L) of 1.0 mm. The step sizes of temporal and spatial discretization in the FE calculations are fine enough for the convergence of the numerical results. Lamb waves are excited by the force function $f(t)$ at x=0, and are received at the point 10 mm away from the superlattices array. The generation source is far from the Fibonacci superlattices in order to obtain approximately plane waves when the wave fronts reach the plate. The received vertical displacement in time domain is Fourier-transformed into the frequency domain to yield the TPS.

We also adopt the HRA to study three quasiperiodic systems. Two Generalized Fibonacci Systems (Type A and Type B) [26] are obtained inductively through the following transformations:

$$A \to AAB,\ B \to A \quad \text{for Type A Fibonacci System} \tag{38a}$$

$$A \to ABB,\ B \to A \quad \text{for Type B Fibonacci System} \tag{38b}$$

We can generate the two quasiperiodic systems, as shown as follows:

$$AABAABAAABAABAAABAAB\ldots \text{ for Type A Fibonacci System} \tag{39a}$$

$$ABBAAABBABBABBAAABBA\ldots \text{ for Type B Fibonacci System} \tag{39b}$$

It is interesting to find out that Generalized Fibonacci Systems are very flexible in forms and by changing the transformations ($A \to ABA$, $B \to A$ …) we can obtain many other quasiperiodic systems.

Then, we can introduce the third quasiperiodic system (Double-period System) into this model. The recursion relation for Double-period System is $A \to AB$, $B \to AA$ [27]. With the recursion relation, we can obtain the sequence of the Double-period System:

$$ABAAABABABAAABAAABAA\ldots \text{for Double-period System} \tag{40}$$

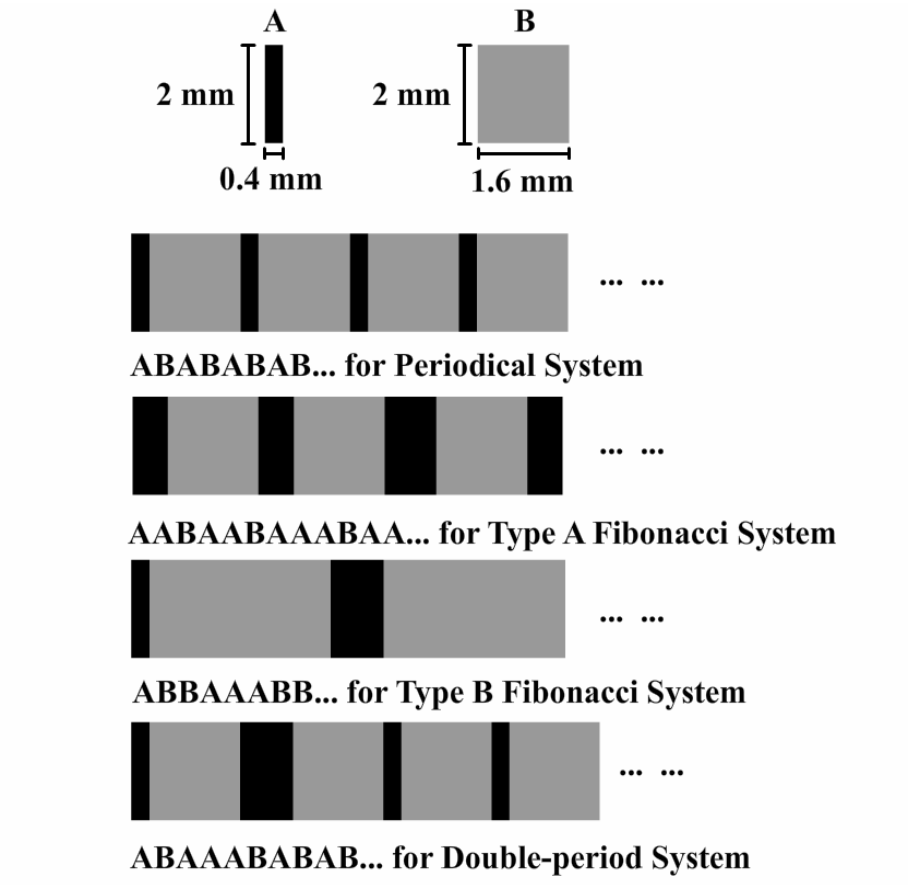

Fig. 6. The schematic diagram of the four systems: Periodic System, Type A Fibonacci System, Type B Fibonacci System and Double-period System, respectively.

Fig. 6 shows the scheme of the four different systems, namely, Periodic System, Type A Fibonacci System, Type B Fibonacci System and Double-period System, respectively. In numerical simulations, the homogeneous media A and B are gold and silicon, with the thicknesses of media A and B are 2 mm, and the widths of media A and B are 0.4 and 1.6 mm, respectively.

3. Lower-order lamb waves in 1D composite thin plates without/with substrate

In order to demonstrate the existence of band gaps for low-order Lamb wave modes in the 1D periodic structure as shown in Fig.1, we have calculated the dispersion curves for a cubic medium (silicon) of a l mm thick plate by considering only the fundamental term in the Fourier and Floquet series [16], as shown in Fig. 7(a). Fig. 7(b) displays the dispersion

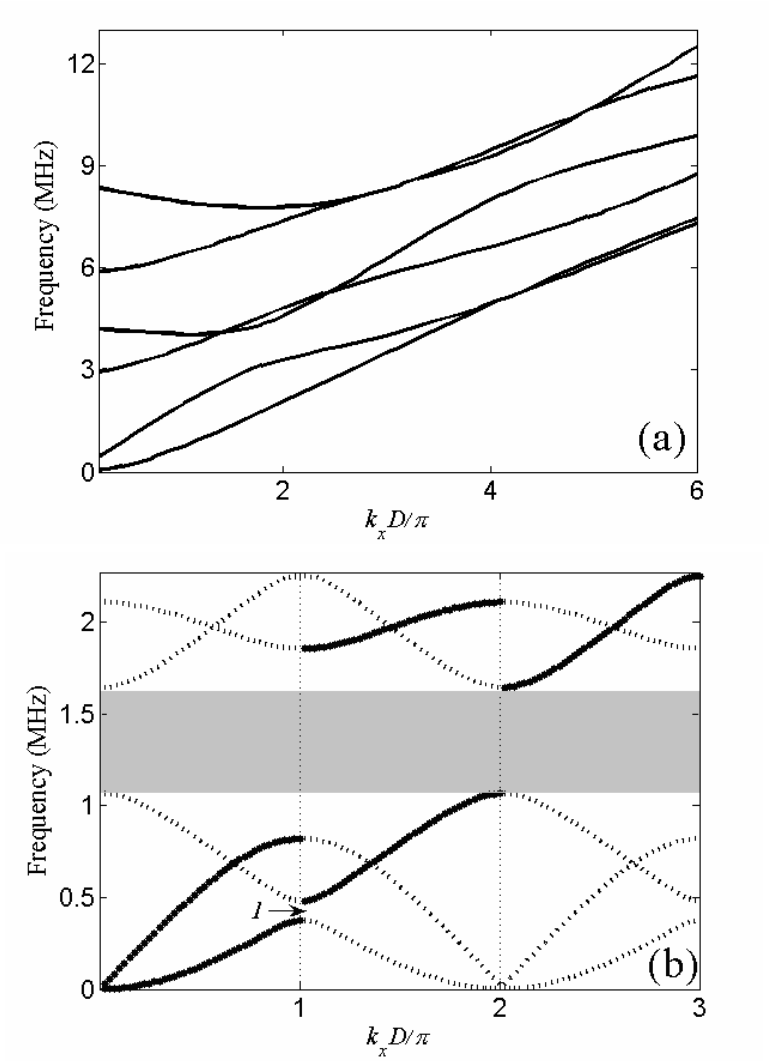

Fig. 7. Schematic representation of the Lamb wave dispersion curve for (a) a homogeneous Si plate with $L = 1.0$ mm (b) composite thin plate (W / Si) with $f = 0.5$, $L = 1.0$ mm, and $D = 2.0$ mm.

curves of four lower-order modes along the boundary of the mini-Brillouin zone with filling ratio $f = 0.5$, $L = 1.0$ mm, and $D = 2.0$ mm. One can obviously observe the modifications produced by resonant reflections in the strip lattice. The dashed vertical line identifies the frequency zone where all the Lamb wave modes are resonantly reflected by the periodic lattice of strips. The proposed approach allows one to identify that the forward propagating Lamb wave modes are not coupled with the backward propagating modes.

By comparing Fig. 7(a) with Fig. 7(b), one can easily find that there exists a band gap from 1065 to 1642 kHz for the lower-order Lamb wave modes propagating in the 1D periodic structure. The gap width ($\Delta\Omega$) is 577 kHz and the corresponding gap/midgap ratio ($\Delta\Omega / \Omega_m$, Ω_m is the midgap frequency) is approximately 0.426. In order to analyze the influence of the ratio L/D for the band gap width, we also calculate the dispersion curves of the lower-order modes with $f = 0.5$, $L = 2.0$ mm, and $D = 2.0$ mm, as shown in Fig. 8. It is apparent that there are two band gaps (from 806 to 1167 kHz and from 1438 to 1863 kHz, respectively) for the ratio $L/D = 1$. The gap widths are 361 and 425 kHz, and the corresponding gap/midgap ratios are about 0.366 and 0.255, respectively.

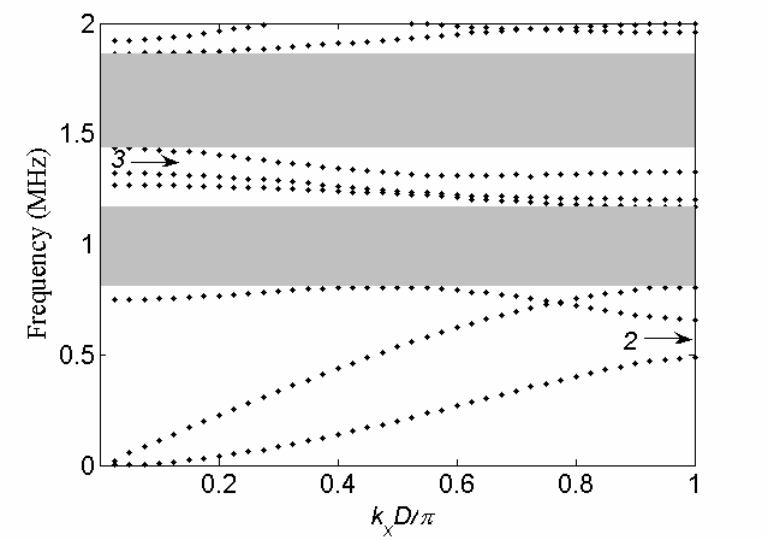

Fig. 8. Dispersion curves of Lamb wave modes for 1D finite thickness composite plate with filling ratio $f = 0.5$, $L = 2.0$ mm, and $D = 2.0$ mm.

Basically, there are three parameters that influence the formation of band gaps, i.e., L/D, f, and the contrast between the physical parameters of the constituents. It is rather intuitive that L/D is very crucial for the formation of a band gap. If it is either too small or too large, there should be no band gaps for lower-order modes. Fig. 9 depicts the gap width of the lowest band gap as a function of L/D with $f = 0.5$ and $D = 2$ mm for tungsten/silicon supperlattices. It is noteworthy to point out that the lowest band gap opens up over a domain of the ratio of L/D defined by $0.15 \le L/D \le 1.64$. The maximum value of gap width appears at $L/D \approx 0.53$ for the lowest band gap and reaches 610 kHz as shown in Fig. 9.

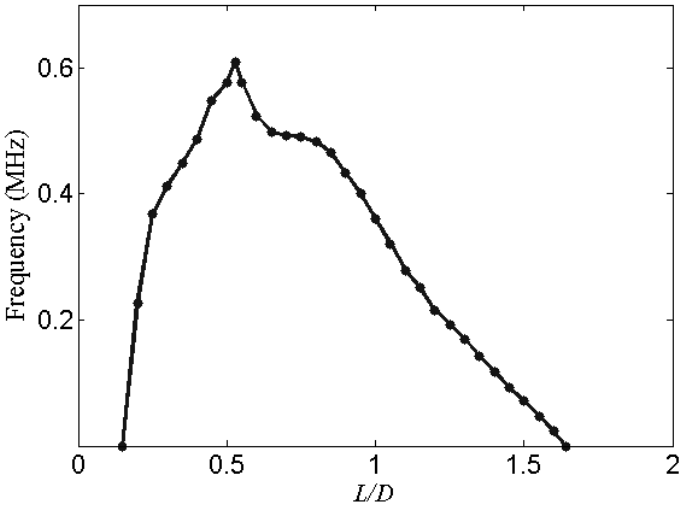

Fig. 9. The width of the lowest band gap at the filling fraction $f = 0.5$ versus the value of L/D.

It is noted that the value of the normalized gap width of the lowest band gap in the systems increases progressively with the increase of the value of the ratio of L/D until a critical value and then decreases. In fact, a plate can support a number of Lamb wave modes depending on the value of the ratio L/λ, where λ is the acoustic wavelength. When the periodicity of these Lamb waves matches the lattice spacing, stop bands appear in the Lamb wave dispersion curves [28]. There is a high interaction when the wavelength of Lamb wave is close the lattice constant, which induces mode conversion and reflections. When the wavelength of Lamb wave is different from the periodicity of the lattice constant, the interaction is weak. On the another hand, the midgap frequency of forbidden gap is inversely proportional to the lattice constant D [29], therefore, the value of the ratio of L/D is important for the width of the band gap for the Lamb waves in the periodic composite systems.

In order to demonstrate further the existence of the band gaps for the lower-order modes in the 1D periodic structure, the finite element method (FEM) is employed to calculate the transmitted power spectra (TPS) for the finite periodic structure as shown in Fig.3.

Fig. 10 shows the TPS for the 1D composite structure plate with $f = 0.5$, $L = 1.0$ mm, and $D = 2.0$ mm. There is a broad region from 1060 to 1630 kHz that is less than –30dB. The result shows good agreement with that by PWE method. The TPS is also depicted in Fig. 10 from a pure Tungsten plate with the same dimensions, and no sharp attenuation in any frequency domain is observed.

For the second sample, f, D, and the configuration are the same with the first one, and only the thickness of the plate is different (L=2 mm). Fig. 11 depicts the TPS for 1D plate with periodic structure and without periodic structure. The frequency range of the gaps of Lamb waves by PWE is almost the same with those of large attenuation in the calculated TPS .The first gap extends from the frequency of 804 up to 1176 kHz and the second from 1436 to 1869 kHz, which are less than –45dB.

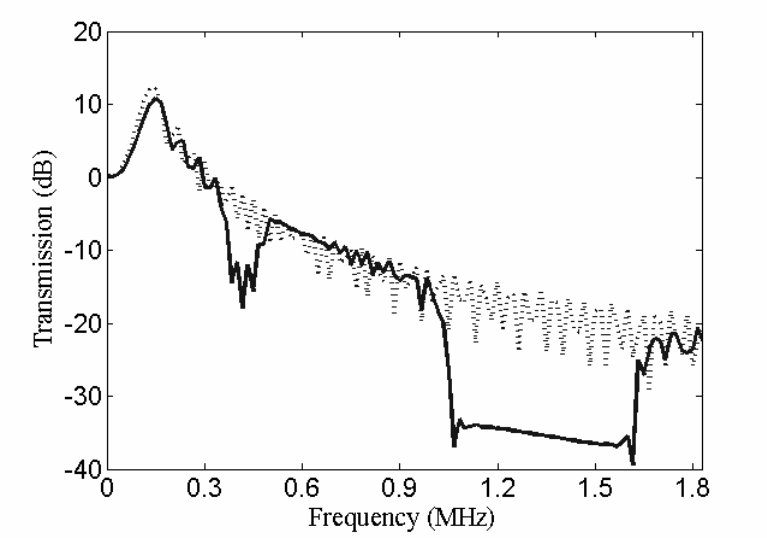

Fig. 10. The TPS computed by the FE method with $f = 0.5$, $L = 1.0$ mm, and $D = 2.0$ mm through the composite pate (solid line) and a pure Tungsten plate (dashed line).

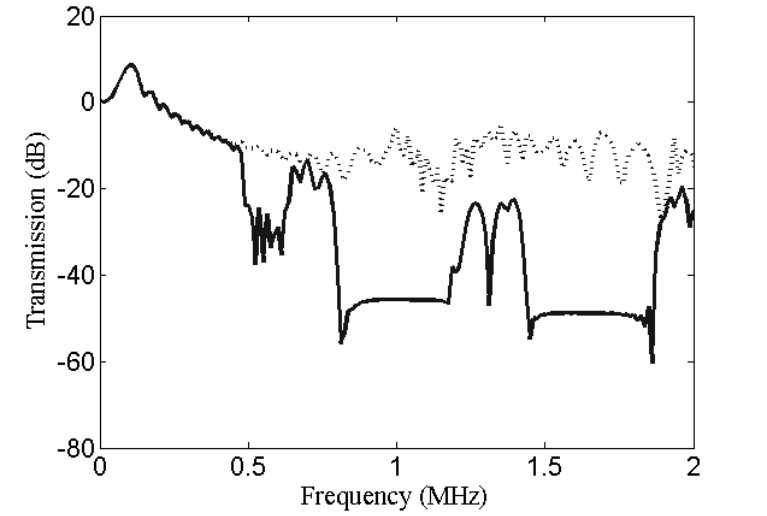

Fig. 11. The TPS computed by the FE method with $f = 0.5$, $L = 2.0$ mm, and $D = 2.0$ mm: through the composite plate (solid line) and through a pure Tungsten plate (dashed line).

It is interesting to notice that there are some slight dips centered at about 0.4MHz in Fig. 6, or 0.5MHz and 1.3MHz in Fig. 11. These dips attribute to the band gaps of antisymmetric modes, but not absolute band gap of both symmetric and antisymmetric modes, which can be observed in Figs. 7(b) and 8, indicated by the arrows 1, 2 and 3. On the other hand, the